General Carrier Index Aided Dual-Mode Differential Chaos Shift Keying with Full Mapping: Design and Optimization

Xiangming Cai, Weikai Xu, *Member, IEEE,* Shaohua Hong, *Member, IEEE,* Lin Wang, *Senior Member, IEEE* Lin Zhang, *Senior Member, IEEE*

***Abstract*—In this paper, we propose a general carrier index assisted dual-mode differential chaos shift keying with full mapping (GCI-DM-DCSK-FM) system, where a pair of distinguishable modem-mode signals is designed with the aid of general carrier index modulation. Specifically, the selected and unselected subcarriers are used to carry differential chaos shift keying (DCSK) and quadrature chaos shift keying (QCSK) signals, respectively, thereby obtaining higher data rate and spectral efficiency. To tackle the issue of discarding the subcarrier activation pattern (SAP), an effective full mapping method is proposed for the GCI-DM-DCSK-FM system to harvest better bit error rate (BER) performance and higher data rate. Moreover, a noise decontamination method is designed for the GCI-DM-DCSK-FM system to enhance the BER performance. To confirm the validness for our proposed systems, we derive the BER expressions of the GCI-DM-DCSK-FM system over additive white Gaussian noise (AWGN) and multipath Rayleigh fading channels. Finally, plenty of simulation results show the excellent BER performance of the GCI-DM-DCSK-FM system.**

***Index Terms*—Chaotic communication, differential chaos shift keying, dual-mode signal, full mapping, noise decontamination.**

I. Introduction

As a kind of noise-like signals, chaotic signals are characterized by the wide-band and good auto-correlation property. Chaotic communication using the chaotic signal as its carrier has gained a significant attention in spread-spectrum (SS) and secure communications [1], [2]. Generally, chaotic communication can be categorized as coherent and non-coherent schemes by judging whether the receiver needs chaotic synchronization [3], [4]. Carroll and Pecora have theoretically and experimentally expounded that it is possible to design synchronizing systems driven by chaotic signals [5], [6]. A deep chaos synchronization scheme using a convolutional neural network (CNN) was proposed in [7] to realize the chaotic synchronization over a noisy channel.

In 1993, Dedieu *et al.* designed a coherent chaos shift keying (CSK) system where its receiver uses the synchronized chaotic signal to retrieve the information bit [8]. However, perfect chaotic synchronization is still an intractable problem [1], [9], [10]. Many researches have proposed non-coherent chaotic communication systems to avoid chaos synchronization. As a diffusely investigated non-coherent chaotic communication scheme, differential chaos shift keying (DCSK) [11] transmits a piece of reference signal before the information bearing signal. In such system, the adverse impact of multipath propagation can be mitigated without the need for channel state information (CSI) [12], [13]. Nevertheless, the data rate and spectral efficiency of DCSK are rather low [14], [15].

In order to achieve higher data rate and spectral efficiency, a quadrature chaos shift keying (QCSK) [16] and general M-ary DCSK [17] utilize the reference signal and its Hilbert transform to modulate the quaternary and M-ary constellations, respectively. In [18], a multilevel code-shifted DCSK with M-ary modulation (MCS-MDCSK) was proposed to obtain a higher data rate. However, a high modulation order penalizes the BER performance of MCS-MDCSK. In addition, a frequency-multiplexed multicarrier DCSK (MC-DCSK) and its enhanced version (referred to as MC-CSK) were proposed in [19] and [20], respectively, to enhance the data rate and energy efficiency. In [21], a multiuser orthogonal frequency division multiplexing (OFDM) assisted DCSK system was proposed where the simple IFFT/FFT operations are used to replace the parallel matched filters in MC-DCSK so that the system complexity can be reduced.

Index modulation (IM) has been widely recognized as a spectral-efficient physical layer solution for 5G and beyond wireless networks over the past few years [22], [23]. Permutation index DCSK (PI-DCSK) [24] and commutation code index DCSK (CCI-DCSK) [25] systems utilize the specific indices of the permuted and commutated reference signals to transmit the additional information bits, respectively. Recently, a dual-mode DCSK with index modulation (DM-DCSK-IM) was proposed in [26] where the index of time slot is regarded as a new transmission entity. Nevertheless, lots of wide-band delay lines are necessary for such configuration, causing the

This work was supported in part by the Natural Science Foundation (NSF) of China under Grant No. 61871337 and 61671395, in part by the NSF of Fujian Province under Grant No. 2020J01003, in part by the NSF of Guangdong Province under Grant No. 2018A030313710, and in part by Key Research and Development and Transformation Plan of Science and Technology Program for Tibet Autonomous Region under Grant No. XZ201901-GB-16.

Xiangming Cai, Weikai Xu and Lin Wang are with the Department of Information and Communication Engineering, Xiamen University, Xiamen, China. (e-mail: samson0102@qq.com, xweikai@xmu.edu.cn, wanglin@xmu.edu.cn).

S. Hong is with the Department of Information and Communication Engineering, Xiamen University 361005, Xiamen, China, and also with the Shenzhen Research Institute of Xiamen University, Shenzhen 518000, China (e-mail: hongsh@xmu.edu.cn).

Lin Zhang is with School of Electronics and Information Technology, Sun Yat-sen University, Guangzhou 510006, China, and is also with the Southern Marine Science and Engineering Guangdong Laboratory, Zhuhai 519000, China (email: isszl@mail.sysu.edu.cn).

dilemma of the implementation-unfriendly hardware in CMOS technology [27].

As a subclass of IM, code index modulation (CIM) was proposed in [28], [29] where information bits are transmitted not only by the physical constellation symbols, but also by the specific indices of spreading codes. The CIM scheme increases the throughput and decreases the energy consumption while keeping the system easy to implement [29]. Many CIM-based DCSK schemes, which integrates the CIM technique with DCSK variants (such as the code-shifted DCSK [30], short reference DCSK [31] and orthogonal multilevel DCSK [32]), were proposed in [33]–[36] to enhance the data rate, spectral efficiency and BER performance.

A multicarrier M-ary orthogonal chaotic vector shift keying with index modulation (MC-MOCVSK-IM) was proposed in [37] where the specific indices of the selected reference signals also serve as an additional dimension to enhance the data rate. In our recent work, a joint time-frequency index keying assisted multiple-mode DCSK (JTFIM-MM-DCSK) [38] system was proposed to achieve high-data-rate communications. Moreover, an M-ary DCSK based on joint carrier-code IM (referred to as JCCIM-MDCSK) was proposed in [39], where the benefits of carrier and spreading code aided IM are fully exploited to enhance system robustness. However, if the receiver detects the discarded subcarrier activation pattern (SAP), MC-MOCVSK-IM, JTFIM-MM-DCSK and JCCIM-MDCSK inevitably suffer from the dramatically deteriorating BER performance. Note that, the BER performances of JTFIM-MM-DCSK depends more heavily on index detection than the general IM-based DCSK systems. It is because all transmission entities (subcarriers and time slots) are used to carry information bits, and once there is an error in index detection, the information bits carried by these entities would be demodulated incorrectly.

The state of whether a subcarrier is activated can also be regarded as a dimension to convey additional bits. For example, Cheng *et al.* proposed a carrier index DCSK (CI-DCSK) [40] system and its M-ary version (CI-MDCSK) [41] to convey the extra bits by the specific indices of the active subcarriers. Specifically, a simple one-to-one mapping between the index symbols and the carrier activation patterns is used in CI-DCSK and CI-MDCSK, which restricts the flexibility and practicality. To address this issue, a general carrier index modulation aided DCSK (GCI-DCSK) system equipped with the flexible numbers of active subcarriers was proposed in [42] where a combinatorial method developed in [43] is used to ascertain the SAP and therefore more mapped bits and modulated bits are transmitted to provide higher data rate and spectral efficiency.

However, the number of possible patterns is a power of two and part of the legitimate SAPs are discarded in GCI-DCSK and JTFIM-MM-DCSK which decreases the data rate and spectral efficiency. Furthermore, the more legitimate SAPs are discarded, the higher the probability of incorrect index detection would be, which leads to the deteriorating BER performance. From another point of view, although the indices of subcarriers are used in GCI-DCSK as a new dimension to carry additional information bits, the inactive subcarriers are null, which means these subcarrier resources are not assigned to transmit any bits, thereby resulting in the unnecessary loss in data rate and spectral efficiency.

Against this background, we propose a general carrier index assisted dual-mode differential chaos shift keying with full mapping (GCI-DM-DCSK-FM) in this paper. In this system, all subcarrier resources are fully exploited in a discernible manner. To cope with the issue related to the mapping relationship of index bits to SAPs (namely part of legitimate SAPs are abandoned), an effective full mapping method is designed for GCI-DM-DCSK-FM. In addition, a noise decontamination method is used in the proposed GCI-DM-DCSK-FM system to improve the BER performance. Different from the existing IM-based DCSK systems, such as DM-DCSK-IM, MC-MOCVSK-IM, JTFIM-MM-DCSK and JCCIM-MDCSK, the GCI-DM-DCSK-FM system makes full use of all SAPs to avoid the performance degradation when the index demodulator detects an invalid SAP. In addition, different from the Walsh-code-based DCSK systems, such as MCS-MDCSK, CIM-CS-DCSK, CIM-DCSK, CIM-MC-MDCSK, CIM-OM-MDCSK and JCCIM-MDCSK, the proposed GCI-DM-DCSK-FM system avoids the synchronization of Walsh codes and thus decreases the hardware overheads. Different from DM-DCSK-IM and JTFIM-MM-DCSK, the problems in the long radio-frequency delay lines are well addressed in the proposed GCI-DM-DCSK-FM system as well.

The main contributions of this paper are as follows:

- We propose a general carrier index assisted dual-mode differential chaos shift keying system with full mapping, which makes full use of the active and inactive subcarriers to enhance the data rate and spectral efficiency.
- We design an effective full mapping method for GCI-DM-DCSK-FM. This method improves the data rate and BER performance without discarding any SAPs. To suppress the adverse effect of channel noise, a noise decontamination method is used in GCI-DM-DCSK-FM to enhance system robustness.
- We derive the BER expressions for GCI-DM-DCSK-FM over AWGN and multipath Rayleigh fading channels which are verified by computer simulations. Substantial simulations show that GCI-DM-DCSK-FM and its noise-decontamination scheme obtain superior BER performance compared to other DCSK-based systems.

The rest of this paper is organized as follow. In Section II, the full mapping method and system model are given. In the same section, we also analyze the data rate, spectral efficiency, energy efficiency and system complexity of GCI-DM-DCSK-FM. After that, performance analysis and optimization are given in Section III and IV, respectively. Section V shows the simulation results while Section VI concludes this paper.

II. The GCI-DM-DCSK-FM System

A. Full Mapping

In the GCI-DCSK system, U out of P subcarriers are activated to produce $\kappa = \binom{P}{U}$ possible SAPs, where $\binom{\cdot}{\cdot}$ denotes the binomial coefficient. Thus, the overall number of mapped bits is calculated as $g_1 = \lfloor \log_2 \kappa \rfloor$, where $\lfloor \cdot \rfloor$ is the floor

TABLE I
THE RELATIONSHIP OF MAPPED BITS TO SAPS WHEN $P = 4$ AND $U = 2$

Mapped bits	SAPs	∂_1	∂_2	ℓ_1	ℓ_2
000	$\Im_1 = \{1, 2\}$	$s_i\mathbf{c}_x$	0	$s_i\mathbf{c}_x$	$a_i\mathbf{c}_x + b_i\mathbf{c}_y$
001	$\Im_2 = \{1, 3\}$	$s_i\mathbf{c}_x$	0	$s_i\mathbf{c}_x$	$a_i\mathbf{c}_x + b_i\mathbf{c}_y$
010	$\Im_3 = \{2, 3\}$	$s_i\mathbf{c}_x$	0	$s_i\mathbf{c}_x$	$a_i\mathbf{c}_x + b_i\mathbf{c}_y$
011	$\Im_4 = \{1, 4\}$	$s_i\mathbf{c}_x$	0	$s_i\mathbf{c}_x$	$a_i\mathbf{c}_x + b_i\mathbf{c}_y$
100	$\Im_5 = \{2, 4\}$	$s_i\mathbf{c}_x$	0	$s_i\mathbf{c}_x$	$a_i\mathbf{c}_x + b_i\mathbf{c}_y$
101	$\Im_6 = \{3, 4\}$	$s_i\mathbf{c}_x$	0	$s_i\mathbf{c}_x$	$a_i\mathbf{c}_x + b_i\mathbf{c}_y$
110	$\Im_7 = \{1, 2\}$	$s_i\mathbf{c}_y$	0	$s_i\mathbf{c}_y$	$a_i\mathbf{c}_x + b_i\mathbf{c}_y$
111	$\Im_8 = \{1, 3\}$	$s_i\mathbf{c}_y$	0	$s_i\mathbf{c}_y$	$a_i\mathbf{c}_x + b_i\mathbf{c}_y$

† ∂_1 and ∂_2 are the transmitted signals within the selected and unselected subcarriers in the GCI-DCSK with full mapping. ℓ_1 and ℓ_2 are the DCSK and QCSK signals in the GCI-DM-DCSK-FM system corresponding to the selected and unselected subcarriers.

function. When taking the combinatorial method [42], [43] into consideration, the overall number of all possible SAPs should be truncated to be a power of two. In other words, only 2^{g_1} SAPs are used and the remaining $\kappa - 2^{g_1}$ patterns are abandoned (see an example in Table I when $P = 4$ and $U = 2$, where the rows with the green shade denote the discarded SAPs), which decreases the data rate. To deal with this dilemma, we propose an effective full mapping method to provide full mapping relationship between the index symbols and SAPs.

In our proposed full mapping method, the total number of mapped bits used to determine the indices of the active subcarriers is $g_1 + 1$. Apart from 2^{g_1} SAPs, the remaining $2^{g_1+1} - 2^{g_1}$ possible patterns are also used to achieve better BER performance. To be specific, the active subcarriers in the former κ SAPs $\{\Im_1, \Im_2, \cdots, \Im_\kappa\}$ ascertained by the combinatorial method are used to carry the DCSK signals in the form of $s_i\mathbf{c}_x$, where $\mathbf{c}_x = [c_{x,1}, c_{x,2}, \cdots, c_{x,\beta}]$ is a β-length chaotic sequence generated by the logistic map $c_{k+1} = 1 - 2c_k^2, k = 1, 2, \cdots$. In contrast, the active subcarriers of the rest $2^{g_1+1} - \kappa$ possible patterns $\{\Im_{\kappa+1}, \Im_{\kappa+2}, \cdots, \Im_{2^{g_1+1}}\}$ (see the rows with the yellow shade in Table I) which are the same as the former $2^{g_1+1} - \kappa$ SAPs of $\{\Im_1, \Im_2, \cdots, \Im_\kappa\}$ are used to transmit the DCSK signals in the form of $s_i\mathbf{c}_y$, where $\mathbf{c}_y$, produced by the Hilbert filter, is orthogonal to $\mathbf{c}_x$.

Table I shows a full mapping relationship for GCI-DCSK with full mapping when $P = 4$ and $U = 2$. It is clearly observed that the first two SAPs are reused to transmit the DCSK signals in the form of $s_i\mathbf{c}_y$, and therefore all legitimate SAPs can be fully utilized. In particular, our proposed full mapping method which provides a full mapping relationship between the mapped bits and SAPs can not only avoid the penalty of BER performance when the index demodulator detects an invalid SAP, but also improve the data rate.

B. System Model

The block diagram of the GCI-DM-DCSK-FM transmitter is shown in Fig. 1. In the GCI-DM-DCSK-FM system, if the total number of information subcarriers is large, the complexity of the combinatorial method is undesirable. Against this background, the multiple subcarriers can be divided into several groups before being modulated in the GCI-DM-DCSK-FM transmitter. The total number of transmitted bits per GCI-DM-DCSK-FM symbol Vg is divided into V groups and each group includes $g = g_1 + 1 + g_2$ bits, where $g_1 + 1$ bits are the mapped bits and g_2 bits are the modulated bits. In addition, the total number of subcarriers is $V(1+P)$, where each group has $1 + P$ subcarriers. Since each group has similar configuration, we only consider one of them for brevity. In the first group, U out of P subcarriers are selected to transmit the DCSK signals, while the remaining $P - U$ signals are used to convey the QCSK signals. Therefore, the number of mapped bits and modulated bits can be calculated as $g_1 + 1 = \lfloor \log_2(\binom{P}{U}) \rfloor + 1$ and $g_2 = U + 2(P - U)$, respectively.

According to the full mapping method, the mapped bits are first loaded into the block of full mapping to produce a corresponding SAP. Secondly, the modulated bits, signals $\mathbf{c}_x$ and $\mathbf{c}_y$ are fed into the dual-mode modulator to form two different kinds of DCSK signals and a QCSK signal and they are expressed as $\mathbf{m}_x = s_i\mathbf{c}_x$, $\mathbf{m}_y = s_i\mathbf{c}_y$ and $\mathbf{m}_z = a_i\mathbf{c}_x + b_i\mathbf{c}_y$, respectively. Table I shows the mapping relationship of mapped bits to SAPs in the GCI-DM-DCSK-FM system when $P = 4$ and $U = 2$. Furthermore, the transmitted DCSK and QCSK signals in the selected and unselected subcarriers are also presented in Table I where $s_i \in \{-\frac{1}{2}, \frac{1}{2}\}$ and $a_i + jb_i \in \{-\frac{\sqrt{2}}{2} + \frac{\sqrt{2}}{2}j, -\frac{\sqrt{2}}{2} - \frac{\sqrt{2}}{2}j, \frac{\sqrt{2}}{2} + \frac{\sqrt{2}}{2}j, \frac{\sqrt{2}}{2} - \frac{\sqrt{2}}{2}j\}$. The resultant discrete signals $\mathbf{m}_x$, $\mathbf{m}_y$ and $\mathbf{m}_z$ are processed by the pulse shaping filters to form the corresponding analog signals, i.e., $m_i(t) = \sum_{k=1}^{\beta} (\mathbf{m}_i)_k h_p(t - kT_c), i \in \{x, y, z\}$, where $(\cdot)_k$ denotes the k^{th} element of $\mathbf{m}_i$ and $h_p(t)$ is the normalized pulse response of a square-root-raised-cosine filter.

The transmitted signal of the GCI-DM-DCSK-FM system can be expressed as

$$e(t) = \sum_{v=1}^{V} \left[c_x(t) \cos(2\pi f_0^v t) + \sum_{p=1}^{P} m_{i,p}^v(t) \cos\left(2\pi f_p^v t\right) \right], \tag{1}$$

where $c_x(t)$ denotes the reference signal, f_0^v and f_p^v are the frequencies of reference and p^{th} information subcarriers corresponding to the v^{th} group. $m_{i,p}^v(t), i \in \{x, y, z\}$ is the DCSK or QCSK signal determined by the SAPs in the v^{th} group. Note that the block following the pulse shaping blocks (i.e., the block with grey shade in Fig. 1) is used to determine the selected subcarriers according to the full mapping method.

After the transmitted signal passes through the multipath Rayleigh fading channel and then the resultant signal is contaminated by an additive white Gaussian noise $n(t)$ with zero mean and $N_0/2$ variance, the received signal is given by

$$r(t) = \sum_{l=1}^{L} \alpha_l e(t - \tau_l) + n(t) \tag{2}$$

where L denotes the number of paths. α_l and τ_l are the channel coefficient and the corresponding delay. When the maximum delay is much less than the symbol period, namely $0 < \tau_l \ll \beta$, the inter-symbol interference (ISI) can be

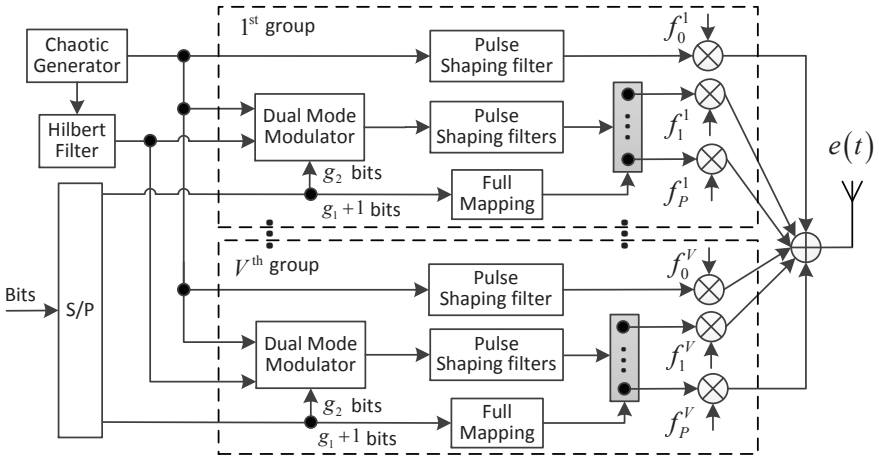

Fig. 1. Block diagram of the GCI-DM-DCSK-FM transmitter.

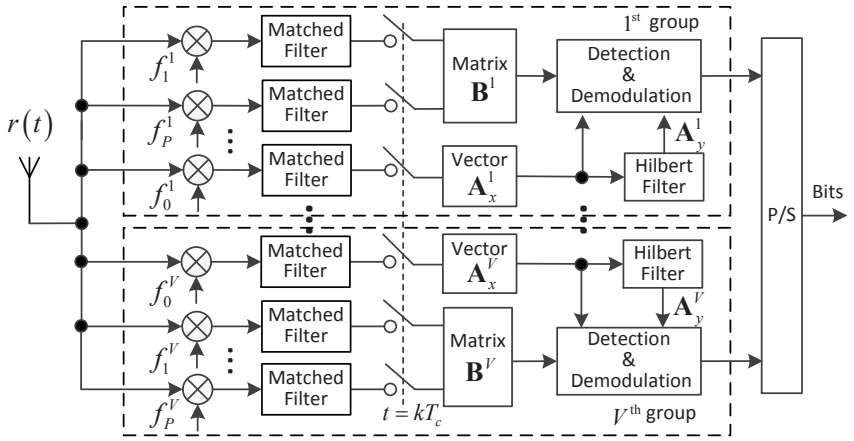

Fig. 2. Block diagram of the GCI-DM-DCSK-FM receiver.

ignored. In addition, it is assumed that the channel coefficients are invariable during a continuous symbol period.

The block diagram of the GCI-DM-DCSK-FM receiver is given in Fig. 2. First, the received signal is multiplied by the synchronized subcarriers to obtain the reference and information bearing signals. After these signals are loaded into the matched filters and then sampled with the interval $t = kT_c$, the resultant discrete signals are stored in vector $(\mathbf{A}_x^v)_{1\times\beta}$ and matrix $(\mathbf{B}^v)_{P\times\beta}$, respectively. In addition, $(\mathbf{A}_y^v)_{1\times\beta}$ is the Hilbert transform of $(\mathbf{A}_x^v)_{1\times\beta}$. Finally, the block of dual-mode detection and demodulation is used to recover the information bits. Specifically, the receiver not only needs to retrieve the modulated bits by demodulating DCSK and QCSK signals, but also needs to get the mapped bits via finding the subcarrier indices of the DCSK signals.

In order to recover the modulated and mapped bits, we propose **Algorithm 1** in this paper. Since the processes of detection and demodulation for different groups are the same, we only need to evaluate one of them. Let $\mathbf{A}^x = \mathbf{A}_x^v$, $\mathbf{A}^y = \mathbf{A}_y^v$ and $\mathbf{B} = \mathbf{B}^v$. At the beginning of the proposed algorithm, the matrix $\mathbf{B}$ is multiplied by $\mathbf{A}^y$, namely $\mathbf{Z}_i^1 = \mathbf{A}^y[\mathbf{B}(i,:)]^T$, where $\mathbf{A}^y$ is orthogonal to $\mathbf{A}^x$, $(\cdot)^T$ is the transpose operation and $\mathbf{B}(i,:)$ denotes the i^{th} row of matrix $\mathbf{B}$. After finding the U minimum elements of $|\mathbf{Z}_i^1|$, the specific SAPs corresponding to these minimum values are determined, i.e., $\{\xi_1, \xi_2, \cdots, \xi_U\}$. Similarly, the specific indices $\{\psi_1, \psi_2, \cdots, \psi_U\}$ corresponding to the U minimum values of $|\mathbf{Z}_i^2|$ can be obtained. In addition, the minimum value of $|\mathbf{Z}_i^1|$ is stored in D_1, while the minimum of $|\mathbf{Z}_i^2|$ is stored in D_2. When $D_1 < D_2$, the SAP is given by $\Im = \{\xi_1, \xi_2, \cdots, \xi_U\}$ and the decision variables of DCSK signals are $\mathbf{J}_i = \mathbf{A}^x[\mathbf{B}(i,:)]^T, i \in \Im$. Otherwise, $\Im = \{\psi_1, \psi_2, \cdots, \psi_U\}$ and $\mathbf{J}_i = \mathbf{A}^y[\mathbf{B}(i,:)]^T, i \in \Im$.

The mapped bits are recovered from the SAP $\Im$ via the reverse full mapping algorithm. After estimating the indices of the selected subcarriers, the dual-mode demodulator knows which subcarriers are used to transmit the DCSK or QCSK signals. In this case, the subcarrier indices of DCSK signals belong to the set $\Im$, while the indices of QCSK signals do not belong to $\Im$. Therefore, the modulated bits are retrieved by the decision variables $\mathbf{J}_i, i \in \Im$ and $\mathbf{K}_i, i \notin \Im$ with the aid of DCSK and QCSK demodulators, respectively.

C. Data Rate and Spectral Efficiency

In order to confirm the superiority of GCI-DM-DCSK-FM, the data rate and spectral efficiency of the proposed system are compared to that of other DCSK-based systems. Since the

Algorithm 1 Recovering Mapped Bits and Modulated Bits

Input: $\mathbf{A}^x$, $\mathbf{A}^y$ and $\mathbf{B}$.

1: **Correlation:** $\mathbf{Z}_i^1 = \mathbf{A}^y[\mathbf{B}(i,:)]^T$, $\mathbf{Z}_i^2 = \mathbf{A}^x[\mathbf{B}(i,:)]^T$, $\mathbf{K}_i = \mathbf{A}^x[\mathbf{B}(i,:)]^T + \sqrt{-1}\mathbf{A}^y[\mathbf{B}(i,:)]^T, i = 1, 2, \cdots, P$.

2: **Search:** Find U minimum values from $\left|\mathbf{Z}_i^1\right|$ and determine the corresponding indices of these minimum values, i.e., $\{\xi_1, \xi_2, \cdots, \xi_U\}$. Meanwhile, the indices of U minimum values, namely $\{\psi_1, \psi_2, \cdots, \psi_U\}$, are determined by finding the U minimum values of $\left|\mathbf{Z}_i^2\right|$. The minimum value of $\left|\mathbf{Z}_i^1\right|$ is stored in D_1, while the minimum of $\left|\mathbf{Z}_i^2\right|$ is stored in D_2.

3: **Judging:**

4: **if** $D_1 < D_2$

5: The SAP is given by $\Im = \{\xi_1, \xi_2, \cdots, \xi_U\}$ and the decision variables of DCSK signals can be expressed as $\mathbf{J}_i = \mathbf{A}^x[\mathbf{B}(i,:)]^T, i \in \Im$.

6: **else**

7: The SAP is given by $\Im = \{\psi_1, \psi_2, \cdots, \psi_U\}$ and the decision variables of DCSK signals can be obtained as $\mathbf{J}_i = \mathbf{A}^y[\mathbf{B}(i,:)]^T, i \in \Im$.

8: **end if**

9: **Recovery:** The mapped bits are recovered from the SAP $\Im$ by the reverse full mapping algorithm. The modulated bits are retrieved by the decision variables $\mathbf{J}_i, i \in \Im$ and $\mathbf{K}_i, i \notin \Im$ with the aid of DCSK and QCSK demodulators.

Output: The mapped bits and modulated bits.

dual-mode signal and full mapping are applied in GCI-DM-DCSK-FM, the data rate of GCI-DM-DCSK-FM is calculated as $R_1 = V[\lfloor \log_2(\binom{P}{U}) \rfloor + 1 + U + 2(P-U)]$. The available data rate of GCI-DCSK is given by $R_2 = V[\lfloor \log_2(\binom{P}{U}) \rfloor + U]$. According to [19], the data rate of the MC-DCSK system is $R_3 = VP$. The data rates of the GCI-DM-DCSK-FM and other chaotic communication systems are shown in Table II. It is clear that GCI-DM-DCSK-FM obtains the highest data rate compared to its competitors.

TABLE II
COMPARISON OF THE DATA RATE

Systems	Data rates
GCI-DM-DCSK-FM	$V[\lfloor \log_2(\binom{P}{U}) \rfloor + 1 + U + 2(P-U)]$
GCI-DCSK	$V[\lfloor \log_2(\binom{P}{U}) \rfloor + U]$
MC-DCSK	VP

Generally, the spectral efficiency is defined as the ratio of bit rate to the total bandwidth in bits/s/Hz. Assuming that the bandwidth of each subcarrier in all systems above is the same and equals B. Therefore, the spectral efficiency of the GCI-DM-DCSK-FM system can be calculated as $\Upsilon_1 = \frac{V[\lfloor \log_2(\binom{P}{U}) \rfloor + 1 + U + 2(P-U)]}{V(P+1)\beta T_c B}$. Similarly, the spectral efficiencies of the GCI-DCSK and MC-DCSK systems are given by $\Upsilon_2 = \frac{V[\lfloor \log_2(\binom{P}{U}) \rfloor + U]}{V(P+1)\beta T_c B}$ and $\Upsilon_3 = \frac{VP}{V(P+1)\beta T_c B}$, respectively. Fig. 3 is plotted to compare the spectral efficiencies of the GCI-DM-DCSK-FM, GCI-DCSK and MC-DCSK systems under the condition of various U. It is shown that the GCI-DM-DCSK-FM system has the best spectral efficiency. In the GCI-DCSK system, parts of SAPs are discarded, which means some subcarrier resources are wasted, thereby resulting in the low spectral efficiency. In contrast, the GCI-DM-DCSK-FM system makes full use of all available subcarriers and all SAPs, thus improving the spectral efficiency significantly.

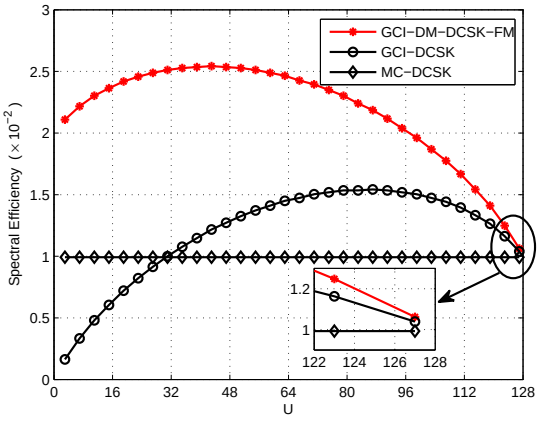

Fig. 3. Comparison of the spectral efficiency between GCI-DM-DCSK-FM and other chaotic communication systems under the condition of $V = 1$, $\beta = 100$, $P = 128$ and various U.

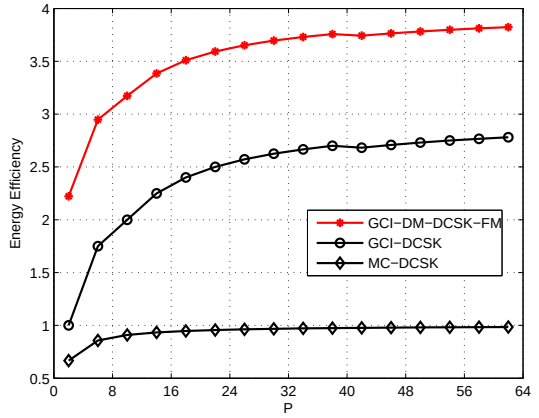

Fig. 4. Comparison of the energy efficiency between GCI-DM-DCSK-FM and other chaotic communication systems. Simulation parameters are $V = 1$ and $U = P/2$.

D. Energy Efficiency and System Complexity

The energy efficiency can be defined as information transmission rate divided by the total transmitted energy. In GCI-DM-DCSK-FM, the symbol energy is calculated as $E_s = V(1 + P - \frac{3}{4}U)\sum_{k=1}^{\beta} \mathrm{E}[c_k^2]$ while the total number of transmitted bits per symbol is $V[\lfloor \log_2(\binom{P}{U}) \rfloor + 1 + U + 2(P-U)]$. It is assumed that the energy of chaotic signal is normalized, i.e., $\sum_{k=1}^{\beta} \mathrm{E}[c_k^2] = 1$. Therefore, the energy efficiency of GCI-DM-DCSK-FM is $\wp_1 = \frac{V[\lfloor \log_2(\binom{P}{U}) \rfloor + 1 + U + 2(P-U)]}{V(1+P-\frac{3}{4}U)}$. According to [42], the energy efficiency of GCI-DCSK is computed as $\wp_2 = \frac{V[\lfloor \log_2(\binom{P}{U}) \rfloor + U]}{V(U+1)}$. In MC-DCSK, part of energy is used to transmit the reference signal and the energy efficiency is

TABLE III
COMPARISON OF SYSTEM COMPLEXITY

Systems	Spreading operations	Despreading operations	Pulse shaping filters	Matched filters	Hilbert filters
GCI-DM-DCSK-FM	$V[U+2(P-U)]$	$2VP$	$V(1+P)$	$V(1+P)$	$1+V$
GCI-DCSK	VU	VP	$V(1+U)$	$V(1+P)$	0
MC-DCSK	VP	VP	$V(1+P)$	$V(1+P)$	0

given by $\wp_3 = \frac{VP}{V(P+1)}$. In Fig. 4, we compare the energy efficiencies of different DCSK-based systems. Clearly, the energy efficiency of GCI-DM-DCSK-FM outperforms that of its competitors especially under the condition of a large P.

System complexity is another important index to evaluate system performance. In GCI-DM-DCSK-FM, the transmitter needs VU and $2V(P-U)$ spreading operations to obtain the DCSK and QCSK signals, respectively. There are $2VP$ despreading operations at the GCI-DM-DCSK-FM receiver. The numbers of spreading, despreading and different filters are shown in Table III. Clearly, the GCI-DM-DCSK-FM system requires more spreading and despreading operations than its competitors. In addition, GCI-DM-DCSK-FM requires $1+V$ Hilbert filters while GCI-DCSK and MC-DCSK do not require the Hilbert filters. Therefore, the system complexity of GCI-DM-DCSK-FM is generally higher than that of GCI-DCSK and MC-DCSK. There is a trade-off between data rate energy efficiency, spectral efficiency and system complexity in GCI-DM-DCSK-FM.

III. PERFORMANCE ANALYSIS

According to the structure of the GCI-DM-DCSK-FM receiver, each group has similar structure. In addition, since the decision variables $\mathbf{Z}_i^1 = \mathbf{A}^y[\mathbf{B}(i,:)]^T$ and $\mathbf{Z}_i^2 = \mathbf{A}^x[\mathbf{B}(i,:)]^T$ are independent of each other, we only need to evaluate one of them. When taking $\mathbf{Z}_i^1 = \mathbf{A}^y[\mathbf{B}(i,:)]^T$ into consideration, there are two different outputs from the correlator. In the first kind of outputs, the selected subcarriers are used to transmit the DCSK signals in the form of $s_i\mathbf{c}_x$ and the corresponding decision variable $Z_{D,i}^1, i=1,2,\cdots,U$ is expressed as

$$Z_{D,i}^1 = \left(\sum_{l=1}^{L}\alpha_l\mathbf{c}_{y,\tau_l}+\mathbf{n}_r\right)\left(\sum_{l=1}^{L}\alpha_l s_i\mathbf{c}_{x,\tau_l}+\mathbf{n}_i\right)^T, \quad (3)$$

where $\mathbf{n}_r$ and $\mathbf{n}_i$ denote the AWGNs imposed on the reference and information bearing signals, respectively. The mean and variance of $Z_{D,i}^1$ are calculated as

$$\mathrm{E}\left[Z_{D,i}^1\right] = 0, \quad (4)$$

$$\begin{aligned}\mathrm{Var}\left[Z_{D,i}^1\right] &= \sum_{l=1}^{L}\alpha_l^2\left(1+\frac{1}{4}\right)\frac{E_s}{V(1+P-\frac{3}{4}U)}\frac{N_0}{2}+\beta\frac{N_0^2}{4}\\ &= \sum_{l=1}^{L}\alpha_l^2\frac{5E_sN_0}{2V\left(4+4P-3U\right)}+\beta\frac{N_0^2}{4}=\sigma_1^2, \quad (5)\end{aligned}$$

where $\mathrm{E}[\cdot]$ and $\mathrm{Var}[\cdot]$ are the mean and variance operations, respectively. $E_s = V(1+P-\frac{3}{4}U)\sum_{k=1}^{\beta}\mathrm{E}[c_k^2]$ denotes the symbol energy of the GCI-DM-DCSK-FM system and $\sum_{k=1}^{\beta}\mathrm{E}[c_k^2]$ is the energy of the chaotic signal.

In terms of the second kind of outputs, the unselected subcarriers are used to transmit the QCSK signals and the decision variable $Z_{Q,i}^1, i=1,2,\cdots,P-U$ is given by

$$Z_{Q,i}^1 = \left[\sum_{l=1}^{L}\alpha_l\mathbf{c}_{y,\tau_l}+\mathbf{n}_r\right]\left[\sum_{l=1}^{L}\alpha_l(a_i\mathbf{c}_{x,\tau_l}+b_i\mathbf{c}_{y,\tau_l})+\mathbf{n}_i\right]^T. \quad (6)$$

The mean and variance of $Z_{Q,i}^1$ are computed as

$$\mathrm{E}\left[Z_{Q,i}^1\right] = \sum_{l=1}^{L}\alpha_l^2\frac{4b_iE_s}{V(4+4P-3U)} = \mu, \quad (7)$$

$$\mathrm{Var}\left[Z_{Q,i}^1\right] = \sum_{l=1}^{L}\alpha_l^2\frac{4E_sN_0}{V(4+4P-3U)}+\beta\frac{N_0^2}{4} = \sigma_2^2. \quad (8)$$

Considering a Gaussian random variable $G\sim N(\mu_g,\sigma_g^2)$, the absolute value of G follows a folded Gaussian distribution whose cumulative distribution function (CDF) and probability density function (PDF) are given, respectively, by [44]

$$\begin{aligned}F_{|G|}(x) &= \frac{1}{2}\left[\mathrm{erf}\left(\frac{x-\mu_g}{\sqrt{2\sigma_g^2}}\right)+\mathrm{erf}\left(\frac{x+\mu_g}{\sqrt{2\sigma_g^2}}\right)\right]\\ &= F_{|G|}\left(\mu_g,\sigma_g^2,x\right), \quad (9)\\ f_{|G|}(x) &= \frac{1}{\sqrt{2\pi\sigma_g^2}}\left\{e^{-\frac{(x-\mu_g)^2}{2\sigma_g^2}}+e^{-\frac{(x+\mu_g)^2}{2\sigma_g^2}}\right\}\\ &= f_{|G|}\left(\mu_g,\sigma_g^2,x\right). \quad (10)\end{aligned}$$

When the maximum absolute value of $Z_{D,i}^1$ is less than the minimum absolute value of $Z_{Q,i}^1$, the indices of the selected subcarriers corresponding to DCSK signals are detected correctly. Let $X=\max\{|Z_{D,i}^1|\}, i=1,2,\cdots,U$ and $Y=\min\{|Z_{Q,i}^1|\}, i=1,2,\cdots,P-U$. The error probability of index symbol is derived as

$$P_d = 1-\Pr\{X<Y\} = 1-\int_0^{\infty}F_X(x)\,f_Y(x)\,\mathrm{d}x, \quad (11)$$

where $F_X(x)$ and $f_Y(x)$ denote the CDF of X and the PDF of Y, respectively. According to [44], $F_X(x)$ and $f_Y(x)$ are given by $F_X(x) = [F_{|Z_{D,i}^1|}(x)]^U$ and $f_Y(x) = (P-U)[1-F_{|Z_{Q,i}^1|}(x)]^{(P-U-1)}f_{|Z_{Q,i}^1|}(x)$, where $F_{|Z_{D,i}^1|}(x) = F_{|Z_{D,i}^1|}(0,\sigma_1^2,x)$, $F_{|Z_{Q,i}^1|}(x) = F_{|Z_{Q,i}^1|}(\mu,\sigma_2^2,x)$ and $f_{|Z_{Q,i}^1|}(x) = f_{|Z_{Q,i}^1|}(\mu,\sigma_2^2,x)$.

After determining the indices of DCSK and QCSK signals, we apply the dual-mode demodulator to retrieve the

TABLE IV
THE DECISION VARIABLES OF DCSK AND QCSK SIGNALS AND THE CORRESPONDING MEANS AND VARIANCES IN THE GCI-DM-DCSK-FM SYSTEM

Signals	Decision variables	Means	Variances
DCSK	$J_i = \left(\sum_{l=1}^{L} \alpha_l \mathbf{c}_{x,\tau_l} + \mathbf{n}_r\right)\left(\sum_{l=1}^{L} \alpha_l s_i \mathbf{c}_{x,\tau_l} + \mathbf{n}_i\right)^T$	$\mathrm{E}[J_i] = \frac{\sum_{l=1}^{L} \alpha_l^2 2E_s}{V(4+4P-3U)}$	$\mathrm{Var}[J_i] = \frac{\sum_{l=1}^{L} \alpha_l^2 5E_s N_0}{2V(4+4P-3U)} + \beta\frac{N_0^2}{4}$
QCSK	$K_i^I = \left[\sum_{l=1}^{L} \alpha_l \mathbf{c}_{x,\tau_l} + \mathbf{n}_r\right]\left[\sum_{l=1}^{L} \alpha_l (a_i \mathbf{c}_{x,\tau_l} + b_i \mathbf{c}_{y,\tau_l}) + \mathbf{n}_i\right]^T$	$\mathrm{E}\left[K_i^I\right] = \frac{\sum_{l=1}^{L} \alpha_l^2 4a_i E_s}{V(4+4P-3U)}$	$\mathrm{Var}\left[K_i^I\right] = \frac{\sum_{l=1}^{L} \alpha_l^2 4E_s N_0}{V(4+4P-3U)} + \beta\frac{N_0^2}{4}$
	$K_i^Q = \left[\sum_{l=1}^{L} \alpha_l \mathbf{c}_{y,\tau_l} + \mathbf{n}_r\right]\left[\sum_{l=1}^{L} \alpha_l (a_i \mathbf{c}_{x,\tau_l} + b_i \mathbf{c}_{y,\tau_l}) + \mathbf{n}_i\right]^T$	$\mathrm{E}\left[K_i^Q\right] = \frac{\sum_{l=1}^{L} \alpha_l^2 4b_i E_s}{V(4+4P-3U)}$	$\mathrm{Var}\left[K_i^Q\right] = \frac{\sum_{l=1}^{L} \alpha_l^2 4E_s N_0}{V(4+4P-3U)} + \beta\frac{N_0^2}{4}$

† Note that K_i^I and K_i^Q denote the in-phase and quadrature branch of K_i in the QCSK signals of the GCI-DM-DCSK-FM System.

modulated bits from DCSK and QCSK signals. The decision variables of DCSK and QCSK signals, and the corresponding means and variances of these decision variables are listed in Table IV. According to [35], the bit error probabilities of DCSK and QCSK signals can be approximated as (12) and (13), as shown at the bottom of this page, where $\gamma_s = \sum_{l=1}^{L} \alpha_l^2 \frac{E_s}{N_0}$ is the symbol signal-to-noise ratio (SNR) and $Q(x) = \frac{1}{\sqrt{2\pi}} \int_x^{+\infty} \exp(-\frac{t^2}{2}) \mathrm{d}t, x \geq 0$.

The overall number of mapped bits in the GCI-DM-DCSK-FM system is $g_1 + 1$, and therefore the BER of mapped bits is given by [24]

$$P_1 = \frac{2^{g_1}}{2^{(g_1+1)} - 1} P_d. \tag{14}$$

The BER of modulated bits is associated with the bit error probability of index symbol P_d, the BERs of DCSK and QCSK signals P_{DCSK} and P_{QCSK}. The BER of modulated bits can be computed as

$$P_2 \approx P_m (1 - P_d) + 0.5 P_d, \tag{15}$$

where $P_m = \frac{U}{U+2(P-U)} P_{DCSK} + \frac{2(P-U)}{U+2(P-U)} P_{QCSK}$. When the transmitted bits are equiprobable, the total BER of the GCI-DM-DCSK-FM system is formulated as

$$\begin{aligned} P_s =& \frac{V(g_1+1)}{V(g_1+1+g_2)} P_1 + \frac{V g_2}{V(g_1+1+g_2)} P_2 \\ =& \frac{\left[\frac{2^{g_1}}{2^{(g_1+1)}-1}(g_1+1) + 0.5 g_2 - g_2 P_m\right] P_d + g_2 P_m}{g_1+1+g_2}. \end{aligned} \tag{16}$$

When the fading channel is modeled as an L-path Rayleigh fading channel, the averaged BER of the GCI-DM-DCSK-FM system over the fading channel is obtained as

$$\bar{P}_s = \int_0^{\infty} P_s \cdot f(\gamma_s) \, \mathrm{d}\gamma_s, \tag{17}$$

where $f(\gamma_s) = \sum_{l=1}^{L} [\frac{1}{\bar{\gamma}_l} (\prod_{j=1, j\neq l}^{L} \frac{\bar{\gamma}_l}{\bar{\gamma}_l - \bar{\gamma}_j}) \exp(-\frac{\gamma_s}{\bar{\gamma}_l})]$ denotes the PDF of the symbol-SNR γ_s and $\bar{\gamma}_l$ is the average value of the instantaneous SNR.

IV. PERFORMANCE OPTIMIZATION

In the GCI-DM-DCSK-FM system, the reference signals collected from different groups can be used to suppress the adverse effect of noises, thereby enhancing the BER performance [45], [46]. At the receiver, the reference signal in the v^{th} group is denoted by $\mathbf{c}_x^v + \mathbf{n}_r^v$, where $\mathbf{n}_r^v$ is the AWGN added in the v^{th} reference signal. To obtain better BER performance, the V reference signals are averaged to produce a new reference signal. The averaging operation decreases the resultant variance of the AWGN by a factor of $1/V$. The averaged reference signal of ND-GCI-DM-DCSK-FM[1] is expressed as

$$\frac{1}{V} \sum_{v=1}^{V} \left(\sum_{l=1}^{L} \alpha_l \mathbf{c}_{x,\tau_l}^v + \mathbf{n}_r^v\right) = \sum_{l=1}^{L} \alpha_l \mathbf{c}_{x,\tau_l} + \mathbf{n}^{\dagger}, \tag{18}$$

where $\mathbf{n}^{\dagger} = \frac{1}{V} \sum_{v=1}^{V} \mathbf{n}_r^v$ is the AWGN with zero mean and $N_0/(2V)$ variance. The Hilbert transform of $\mathbf{n}^{\dagger}$ is given by $\tilde{\mathbf{n}}^{\dagger}$, having the same mean and variance as $\mathbf{n}^{\dagger}$. The decision variables $Z_{D,i}^1, i = 1, 2, \cdots, U$ and $Z_{Q,i}^1, i = 1, 2, \cdots, P-U$ can be rewritten as

$$Z_{D,i}^1 = \left(\sum_{l=1}^{L} \alpha_l \mathbf{c}_{y,\tau_l} + \tilde{\mathbf{n}}^{\dagger}\right)\left(\sum_{l=1}^{L} \alpha_l s_i \mathbf{c}_{x,\tau_l} + \mathbf{n}_i\right)^T, \tag{19}$$

$$Z_{Q,i}^1 = \left[\sum_{l=1}^{L} \alpha_l \mathbf{c}_{y,\tau_l} + \tilde{\mathbf{n}}^{\dagger}\right]\left[\sum_{l=1}^{L} \alpha_l (a_i \mathbf{c}_{x,\tau_l} + b_i \mathbf{c}_{y,\tau_l}) + \mathbf{n}_i\right]^T. \tag{20}$$

[1]In this paper, the GCI-DM-DCSK-FM system with noise decontamination is denoted by the ND-GCI-DM-DCSK-FM system.

$$P_{DCSK} \approx \frac{1}{2}\mathrm{erfc}\left[\left(\frac{2\mathrm{Var}[J_i]}{(\mathrm{E}[J_i])^2}\right)^{-\frac{1}{2}}\right] = \frac{1}{2}\mathrm{erfc}\left[\left(\frac{5V(4+4P-3U)}{4\gamma_s} + \frac{\beta V^2 (4+4P-3U)^2}{8\gamma_s^2}\right)^{-\frac{1}{2}}\right] \tag{12}$$

$$P_{QCSK} \approx Q\left(\frac{\pi \mathrm{E}\left[K_i^I\right]}{4a_i\sqrt{\mathrm{Var}\left[K_i^I\right]}}\right) = Q\left[\left(\frac{4V(4+4P-3U)}{\pi^2\gamma_s} + \frac{\beta V^2 (4+4P-3U)^2}{4\pi^2\gamma_s^2}\right)^{-\frac{1}{2}}\right] \tag{13}$$

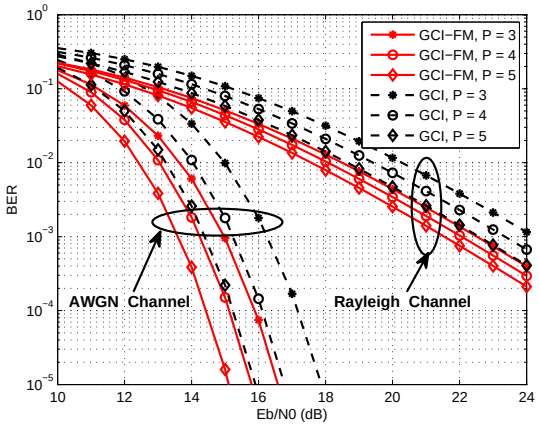

Fig. 5. BER performance comparison between the GCI-DCSK with full mapping and ordinary GCI-DCSK system over AWGN and multipath Rayleigh fading channels. $P = 3, 4, 5$, $U = 2$ and $\beta = 200$.

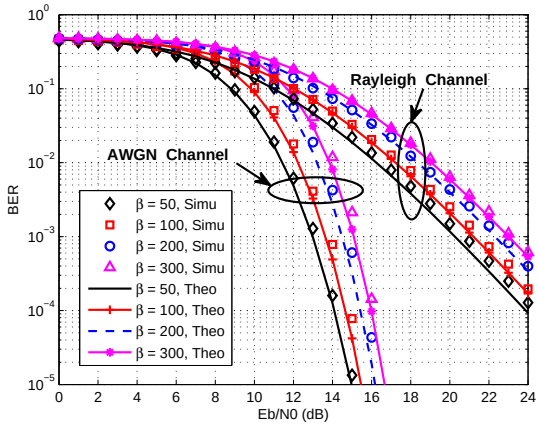

Fig. 6. BER performance of the GCI-DM-DCSK-FM system over AWGN and multipath Rayleigh fading channels. $\beta = 50, 100, 200, 300$, $V = 1$, $P = 4$ and $U = 2$.

The means and variances of $Z^1_{D,i}$ and $Z^1_{Q,i}$ are calculated as

$$\mathrm{E}\left[Z^1_{D,i}\right] = 0, \tag{21}$$

$$\mathrm{Var}\left[Z^1_{D,i}\right] = \sum_{l=1}^{L} \alpha_l^2 \frac{(4V+1)\,E_s N_0}{2V^2(4+4P-3U)} + \beta\frac{N_0^2}{4V} = \sigma_3^2, \tag{22}$$

$$\mathrm{E}\left[Z^1_{Q,i}\right] = \sum_{l=1}^{L} \alpha_l^2 \frac{4 b_i E_s}{V(4+4P-3U)} = \mu, \tag{23}$$

$$\mathrm{Var}\left[Z^1_{Q,i}\right] = \sum_{l=1}^{L} \alpha_l^2 \frac{2\,(V+1)\,E_s N_0}{V^2(4+4P-3U)} + \beta\frac{N_0^2}{4V} = \sigma_4^2. \tag{24}$$

According to (11), the probability of the erroneous index detection can be calculated as

$$P_d = 1 - \int_0^{\infty} \left[F_{|Z^1_{D,i}|}(0, \sigma_3^2, x)\right]^U (P-U) \times \left[1 - F_{|Z^1_{Q,i}|}(\mu, \sigma_4^2, x)\right]^{(P-U-1)} f_{|Z^1_{Q,i}|}(\mu, \sigma_4^2, x)\mathrm{d}x. \tag{25}$$

When the updated reference signal is used to demodulate the modulated bits carried by the DCSK and QCSK signals, the decision variables are given by $I_i = (\sum_{l=1}^{L} \alpha_l \mathbf{c}_{x,\tau_l} + \mathbf{n}^\dagger)(\sum_{l=1}^{L} \alpha_l s_i \mathbf{c}_{x,\tau_l} + \mathbf{n}_i)^T$ and $W_i^I = (\sum_{l=1}^{L} \alpha_l \mathbf{c}_{x,\tau_l} + \mathbf{n}^\dagger)(\sum_{l=1}^{L} \alpha_l (a_i \mathbf{c}_{x,\tau_l} + b_i \mathbf{c}_{y,\tau_l}) + \mathbf{n}_i)^T$, where I_i and W_i^I are the decision variable for the DCSK signal and in-phase branch of the QCSK signal, respectively. The mean and variance of I_i can be calculated as $\mathrm{E}[I_i] = \sum_{l=1}^{L} \alpha_l^2 \frac{2E_s}{V(4+4P-3U)}$ and $\mathrm{Var}[I_i] = \sum_{l=1}^{L} \alpha_l^2 \frac{(4V+1)E_s N_0}{2V^2(4+4P-3U)} + \beta\frac{N_0^2}{4V}$, respectively, In addition, the mean and variance of W_i^I are computed as $\mathrm{E}[W_i^I] = \sum_{l=1}^{L} \alpha_l^2 \frac{4a_i E_s}{V(4+4P-3U)}$ and $\mathrm{Var}[W_i^I] = \sum_{l=1}^{L} \alpha_l^2 \frac{2(V+1)E_s N_0}{V^2(4+4P-3U)} + \beta\frac{N_0^2}{4V}$. Therefore, when the index detection is correct, the BERs of the DCSK and QCSK signals are computed as

$$P_{DCSK} \approx \frac{1}{2}\mathrm{erfc}\left[\left(\frac{(4V+1)\,(4+4P-3U)}{4\gamma_s} + \frac{\beta V(4+4P-3U)^2}{8\gamma_s^2}\right)^{-\frac{1}{2}}\right], \tag{26}$$

$$P_{QCSK} \approx Q\left[\left(\frac{2\,(V+1)\,(4+4P-3U)}{\pi^2\gamma_s} + \frac{\beta V(4+4P-3U)^2}{4\pi^2\gamma_s^2}\right)^{-\frac{1}{2}}\right]. \tag{27}$$

Finally, the bit error probability of the ND-GCI-DM-DCSK-FM system is obtained by substituting (25), (26) and (27) into (16).

V. Numerical Results and Discussions

In this section, computer simulations are performed to validate the advantages of the proposed full mapping method. Moreover, the superiority of the GCI-DM-DCSK-FM system is confirmed via our simulations. Unless otherwise specified, a three-path Rayleigh fading channel with different power coefficients $\mathrm{E}\left(\lambda_1^2\right) = 6/10$, $\mathrm{E}\left(\lambda_2^2\right) = 3/10$ and $\mathrm{E}\left(\lambda_3^2\right) = 1/10$ is adopted in our simulations. The channel delay follows a uniform distribution varying from 0 to $6T_c$. "Simu" and "Theo" denote the simulation and theoretical results, respectively.

As shown in Fig. 5, the BER performance of the GCI-DCSK with full mapping is compared with that of the GCI-DCSK system. The labels "GCI-FM" and "GCI" denote the GCI-DCSK with full mapping and GCI-DCSK systems, respectively. The BER performances of both systems are improved with the increase of P. The GCI-DCSK-FM system with $P = 3$ harvests more than 1dB performance gain over the GCI-DCSK system at the BER level of 10^{-5} in the AWGN channel. Furthermore, the improvement in BER performance is almost 2dB at a BER level 10^{-3} in the Rayleigh fading channel.

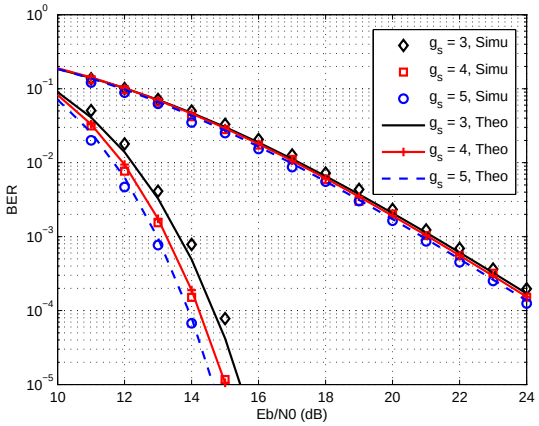

Fig. 7. BER performance of the GCI-DM-DCSK-FM system with $\beta = 100$, $V = 1$ and various g_s over AWGN and multipath Rayleigh fading channels.

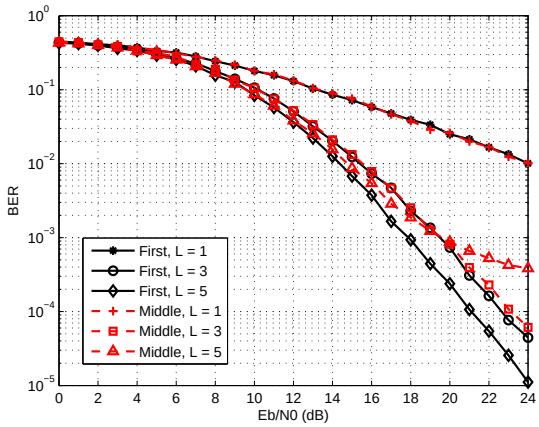

Fig. 8. The effect of reference signal locations on the BER performance of GCI-DM-DCSK-FM over the fading channel. Simulation parameters are $P = 4$, $U = 2$, $\beta = 50$ and $V = 1$.

Since all SAPs are sufficiently exploited in GCI-DCSK-FM, the penalty of BER performance when the index demodulator detects an illegal SAP can be avoided to a great extent.

In Fig. 6, the influence of spreading factor β on the BER performance of the GCI-DM-DCSK-FM system is investigated. As β increases from 50 to 300, the BER performance of the GCI-DM-DCSK-FM system is deteriorating gradually. This is chiefly because the cross-correlation of the noise-to-noise term involved in the decision variable becomes large when β increases. In addition, the effect of the number of mapped bits on the BER performance of the GCI-DM-DCSK-FM system is presented in Fig. 7. The overall number of mapped bits $g_s = g_1 + 1$ is computed as $g_s = 3$, $g_s = 4$ and $g_s = 5$ when $P = 4$, $U = 2$, $P = 6$, $U = 4$ and $P = 8$, $U = 6$, respectively. As g_s increases, the BER performance of the GCI-DM-DCSK-FM system is improved in a moderate manner. For instance, the GCI-DM-DCSK-FM with $g_s = 5$ offers about 1dB gain over $g_s = 3$ at the BER 10^{-5} in the AWGN channel.

In Fig. 8, we study the effect of reference signal locations on the BER performance of GCI-DM-DCSK-FM. In simulations, an L-path Rayleigh fading channel [47] is used where the channel coefficients are given by $\mathrm{E}[\alpha_l] = e^{-0.4(l-1)}, l = 1, 2, \cdots, L$ and then these coefficients are normalized, and the channel delay of each path relative to the previous one is set to 3. The label "First" and "Middle" denote the reference signal is transmitted at the first frequency and at the middle frequency, respectively. As shown in Fig. 8, when $L = 1$ and $L = 3$, the location of the reference signal has little impact on the BER performance of GCI-DM-DCSK-FM. However, when $L = 5$, the BER performance of GCI-DM-DCSK-FM depends heavily on the location of the reference signal. Specifically, GCI-DM-DCSK-FM reaches an error floor when the reference signal is arranged at the middle of subcarriers. It is because the inter-subcarrier interference has a greater influence on the middle subcarrier compared to the marginal one.

As shown in Fig. 9, the BER performance of the ND-GCI-DM-DCSK-FM system with different V is studied over the multipath Rayleigh fading channel. Clearly, the analytical BERs are in a good agreement with the simulated ones. Note

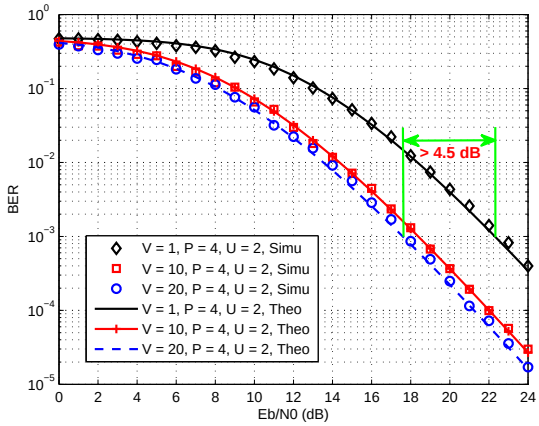

Fig. 9. BER performance of the ND-GCI-DM-DCSK-FM system with $\beta = 200$, $P = 4$, $U = 2$ and different V over the multipath Rayleigh fading channel.

that, when $V = 1$, the ND-GCI-DM-DCSK-FM system is the same as the GCI-DM-DCSK-FM system. With the aid of noise decontamination, the ND-GCI-DM-DCSK-FM system can achieve better BER performance. Specifically, the ND-GCI-DM-DCSK-FM system with $V = 20$ obtains more than 4.5dB performance gain over that of $V = 1$ at the BER level of 10^{-3}.

Moreover, the effect of maximum channel delay τ_2 on the BER performance of the ND-GCI-DM-DCSK-FM system is plotted in Fig. 10. In the performance analysis, it is assumed that the maximum channel delay is much less than the spreading factor. Therefore, the theoretical curves match the simulated ones when τ_2 is small. When the maximum channel delay increases, the BER performance of the ND-GCI-DM-DCSK-FM system gradually degrades, due to the negative effect of ISI. On the other hand, it is clearly observed that the ND-GCI-DM-DCSK-FM system with $V = 20$ is more sensitive to the channel delay than $V = 1$.

The BER performances of GCI-DM-DCSK-FM, MC-DCSK and MC-CSK systems are shown in Fig. 11. The overall

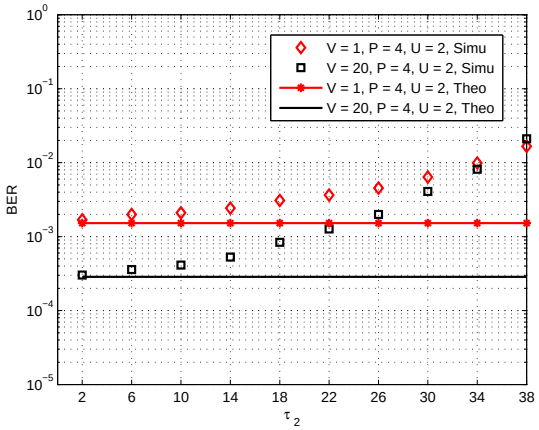

Fig. 10. The effect of maximum channel delay τ_2 on the BER performance of the ND-GCI-DM-DCSK-FM system with $\beta = 50$, $P = 4$, $U = 2$ and different V over the two-path multipath Rayleigh fading channel. The channel coefficients are $\mathrm{E}\left(\lambda_1^2\right) = 1/2$ and $\mathrm{E}\left(\lambda_2^2\right) = 1/2$.

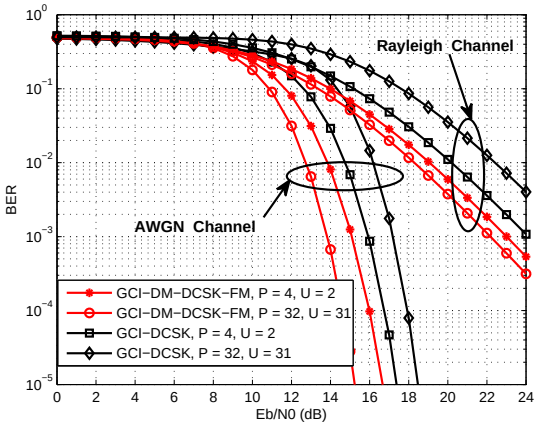

Fig. 12. BER performance comparison between GCI-DM-DCSK-FM and GCI-DCSK systems with $\beta = 300$ and $V = 1$ over AWGN and multipath Rayleigh fading channels.

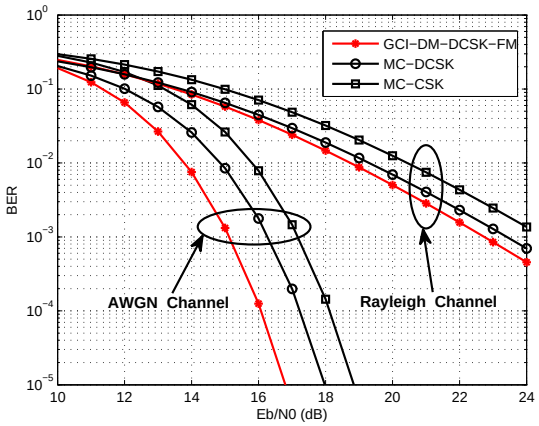

Fig. 11. BER performance comparison of GCI-DM-DCSK-FM, MC-DCSK and MC-CSK systems with the same number of subcarriers $N_s = 4$ and $\beta = 300$ over AWGN and multipath Rayleigh fading channels.

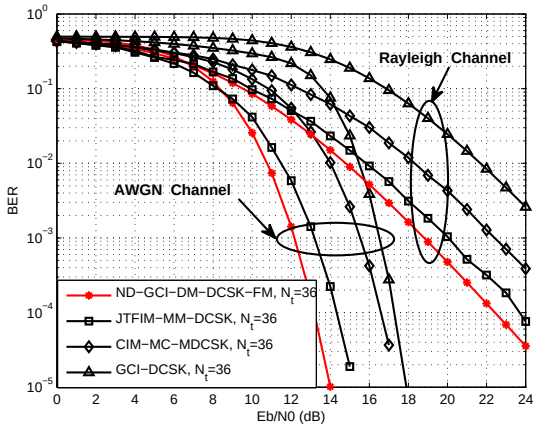

Fig. 13. BER performance comparison between ND-GCI-DM-DCSK-FM and other chaotic communication systems with $\beta = 200$ and same number of transmitted bits per symbol $N_t = 36$ over AWGN and multipath Rayleigh fading channels.

number of subcarriers in all systems is the same, namely $N_s = 4$. The GCI-DM-DCSK-FM system uses $V = 1$, $P = 3$ and $U = 2$ in its simulation. In the AWGN channel, the required E_b/N_0 of the MC-CSK system is closed to 19dB at a BER 10^{-5}, while the GCI-DM-DCSK-FM system only needs less than 17dB to obtain the same BER. Therefore, the GCI-DM-DCSK-FM system obtains about 2dB gain over the MC-CSK system. It is because the GCI-DM-DCSK-FM system not only harvests the benefit of index modulation, but also make full use of the full mapping without discarding any SAPs, which improves the accuracy of index detection.

Furthermore, Fig. 12 is plotted to compare the BER performance of GCI-DM-DCSK-FM with that of GCI-DCSK. It is worth noting that when the number of the selected subcarriers is relatively small (i.e., $U = 2$), the performance gain of the GCI-DM-DCSK-FM system over the GCI-DCSK system is about 1dB at a BER level of 10^{-3} in the AWGN channel. However, when $U = 31$, the performance gain would increase to more than 3dB at the same BER level. It is chiefly due to that the probability of incorrect index detection enlarges in the GCI-DCSK system when U increases from 2 to 31. In contrast, the GCI-DM-DCSK-FM system gets rid of this restriction and harvests better performance.

In Fig. 13, the BER performance of ND-GCI-DM-DCSK-FM is compared to that of its competitors over different channels. The number of the transmitted bits per symbol is identical for all systems and it has been set as $N_t = 36$. In simulations, $P = 4$, $U = 2$ and $V = 4$ are used in ND-GCI-DM-DCSK-FM while $P = 32$ and $U = 31$ are used in GCI-DCSK. In CIM-MC-MDCSK, the order of Walsh code is set to 16 and the modulation order is set to 4. In JTFIM-MM-DCSK, 1 of 2 information-bearing subcarriers is selected to carry the dual-mode signal while 10 of 11 time slots are selected to carry the QCSK signals. As shown in Fig. 13, the best BER performance is achieved by ND-GCI-DM-DCSK-FM and its gains in BER performance over JTFIM-MM-DCSK and CIM-MC-MDCSK are about 1dB and 3.5dB, respectively, at 10^{-4} BER level in the AWGN channel.

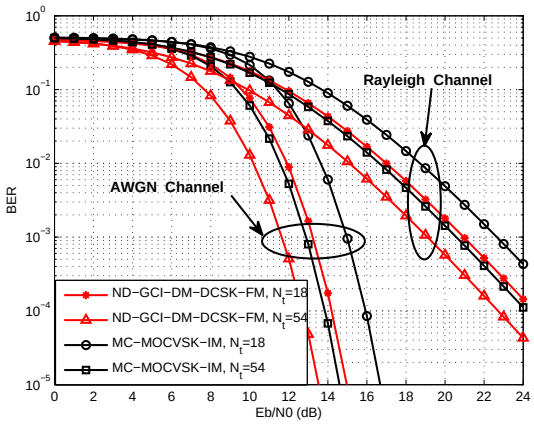

Fig. 14. BER performance comparison between ND-GCI-DM-DCSK-FM and MC-MOCVSK-IM systems with $\beta = 200$ and same number of transmitted bits $N_t = 18, 54$ over AWGN and multipath Rayleigh fading channels.

Finally, the BER performance of the ND-GCI-DM-DCSK-FM system is compared to that of the MC-MOCVSK-IM system under the condition of same transmitted bits $N_t = 18, 54$. In simulations, $P = 4$, $U = 2$ and $V = 2, 6$ are used for ND-GCI-DM-DCSK-FM. In addition, the simulation parameters of MC-MOCVSK-IM are $N_r = 4$, $U_r = 2$, $W_r = 3, 9$ and $M_r = 4$, where N_r is the number of reference signals, U_r is the number of the selected reference signals, W_r is the number of groups of the information bearing signals and M_r is the modulation order. It can be observed from Fig. 14 that when $N_t = 18$, the ND-GCI-DM-DCSK-FM system can obtain about 2dB performance gain in contrast to the MC-MOCVSK-IM system at the BER level of 10^{-5} in the AWGN channel.

VI. Conclusion

A general carrier index assisted dual-mode differential chaos shift keying with full mapping has been proposed in this paper. In this configuration, the effective full mapping method, which provides full mapping without discarding any SAPs, is designed for the GCI-DM-DCSK-FM system to harvest the benefits of higher data rate and better BER performance. Furthermore, in order to further improve the BER performance, a noise decontamination method is used in the GCI-DM-DCSK-FM system to reduce the adverse effect of noises in the reference signals. The analytical BER expressions are derived for the proposed GCI-DM-DCSK-FM system over the AWGN and multipath Rayleigh fading channels. The higher data rate, spectral efficiency, energy efficiency and superior BER performance of the GCI-DM-DCSK-FM system are validated by a mass of comparison results. However, these improvements are at the cost of high system complexity. The proposed GCI-DM-DCSK-FM system and its noise-reducing scheme have 1 to 3dB gain in BER performance compared to its competitors.

References

[1] Y. Fang, G. Han, P. Chen, F. C. M. Lau, G. Chen, and L. Wang, "A survey on DCSK-based communication systems and their application to UWB scenarios," *IEEE Commun. Surveys Tuts.*, vol. 18, no. 3, pp. 1804-1837, 3rd Quart., 2016.

[2] F. C. M. Lau and C. K. Tse, *Chaos-Based Digital Communication Systems: Chaos-Based Digital Communication Systems*. Berlin, Germany: Springer-Verlag, 2003.

[3] H. Yang and G. Jiang, "High-efficiency differential-chaos-shift-keying scheme for chaos-based noncoherent communication," *IEEE Trans. Circuits Syst., II, Exp. Briefs*, vol. 59, no. 5, pp. 312-316, May 2012.

[4] H. Yang and G. Jiang, "Reference-modulated DCSK: A novel chaotic communication scheme," *IEEE Trans. Circuits Syst., II, Exp. Briefs*, vol. 60, no. 4, pp. 232-236, April 2013.

[5] T. L. Carroll and L. M. Pecora, "Synchronizing chaotic circuits," *IEEE Trans. Circuits Syst.*, vol. 38, no. 4, pp. 453-456, April 1991.

[6] L. M. Pecora and T. L. Carroll, "Synchronized chaotic signals and systems," in *1992 IEEE International Conference on Acoustics, Speech, and Signal Processing*, San Francisco, CA, USA, 1992, pp. 137-140 vol.4.

[7] M. Mobini and G. Kaddoum, "Deep Chaos Synchronization," *IEEE Open J. Commun. Soc.*, vol. 1, pp. 1571-1582, 2020.

[8] H. Dedieu, M. P. Kennedy, and M. Hasler, "Chaos shift keying: Modulation and demodulation of a chaotic carrier using self-synchronizing Chua's circuits," *IEEE Trans. Circuits Syst. II, Analog Digit. Signal Process.*, vol. 40, no. 10, pp. 634C642, Oct. 1993.

[9] G. Kolumbán, M. P. Kennedy and L. O. Chua, "The role of synchronization in digital communications using chaos. I . Fundamentals of digital communications," *IEEE Trans. Circuits Syst. I, Fundam. Theory Appl.*, vol. 44, no. 10, pp. 927-936, Oct. 1997.

[10] G. Kolumbán, M. P. Kennedy and L. O. Chua, "The role of synchronization in digital communications using chaos. II. Chaotic modulation and chaotic synchronization," *IEEE Trans. Circuits Syst. I, Fundam. Theory Appl.*, vol. 45, no. 11, pp. 1129-1140, Nov. 1998.

[11] G. Kolumbán, G. K. Vizvári, W. Schwarz, and A. Abel, "Differential chaos shift keying: A robust coding for chaos communication," in *Proc. Nonlinear Dyn. Electron. Syst.*, Seville, Spain, Jun. 1996, pp. 92-97.

[12] M. Dawa, G. Kaddoum, and Z. Sattar, "A generalized lower bound on the bit error rate of DCSK systems over multi-path rayleigh fading channels," *IEEE Trans. Circuits Sys. II, Express Briefs*, vol. 65, no. 3, pp. 321-325, Mar. 2018.

[13] M. Dawa, G. Kaddoum, and M. Herceg, "A framework for the lower bound on the BER of DCSK systems over multi-path Nakagami-m fading channels," *IEEE Trans. Circuits Sys. II, Express Briefs*, vol. 67, no. 10, pp. 1859-1863, Oct. 2020.

[14] M. Qian, G. Cai, Y. Fang and G. Han, "Design of link-selection strategies for buffer-aided DCSK-SWIPT relay system," *IEEE Trans. Commun.*, vol. 68, no. 10, pp. 6023-6038, Oct. 2020.

[15] H. Ma, G. Cai, Y. Fang, P. Chen and G. Chen, "Design of a superposition coding PPM-DCSK system for downlink multi-user transmission," *IEEE Trans. Veh. Technol.*, vol. 69, no. 2, pp. 1666-1678, Feb. 2020.

[16] Z. Galias and G. M. Maggio, "Quadrature chaos-shift keying: Theory and performance analysis," *IEEE Trans. Circuits Syst. I, Fundam. Theory Appl.*, vol. 48, no. 12, pp. 1510-1519, Dec. 2001.

[17] L. Wang, G. Cai, and G. Chen, "Design and performance analysis of a new multiresolution M-ary differential chaos shift keying communication system," *IEEE Trans. Wireless Commun.*, vol. 14, no. 9, pp. 5197-5208, Sept. 2015.

[18] X. Cai, W. Xu, R. Zhang and L. Wang, "A multilevel code shifted differential chaos shift keying system with M-ary modulation," *IEEE Trans. Circuits Syst. II, Exp. Briefs.*, vol. 66, no. 8, pp. 1451-1455, Aug. 2019.

[19] G. Kaddoum, F. Richardson and F. Gagnon, "Design and analysis of a multi-carrier differential chaos shift keying communication system," *IEEE Trans. Commun.*, vol. 61, no. 8, pp. 3281-3291, August 2013.

[20] H. Yang, W. K. S. Tang, G. Chen and G. Jiang, "Multi-carrier chaos shift keying: System design and performance analysis," *IEEE Trans. Circuits Syst. I, Reg. Papers*, vol. 64, no. 8, pp. 2182-2194, Aug. 2017.

[21] G. Kaddoum, "Design and performance analysis of a multiuser OFDM based differential chaos shift keying communication system," *IEEE Trans. Commun.*, vol. 64, no. 1, pp. 249-260, Jan. 2016.

[22] E. Basar, "Index modulation techniques for 5G wireless networks," *IEEE Communications Magazine*, vol. 54, no. 7, pp. 168-175, July 2016.

[23] E. Basar, M. Wen, R. Mesleh, M. Di Renzo, Y. Xiao and H. Haas, "Index modulation techniques for next-generation wireless networks," *IEEE Access*, vol. 5, pp. 16693-16746, 2017.

[24] M. Herceg, G. Kaddoum, D. Vranješ, and E. Soujeri, "Permutation index DCSK modulation technique for secure multiuser high-data-rate communication systems," *IEEE Trans. Veh. Technol.*, vol. 67, no. 4, pp. 2997-3011, Apr. 2018.

[25] M. Herceg, D. Vranješ, G. Kaddoum, and E. Soujeri, "Commutation code index DCSK modulation technique for high-data-rate communication systems," *IEEE Trans. Circuits Syst., II, Exp. Briefs*, vol. 65, no. 12, pp. 1954-1958, Dec. 2018.

[26] X. Cai, W. Xu, S. Hong and L. Wang, "Dual-mode differential chaos shift keying with index modulation," *IEEE Trans. Commun.*, vol. 67, no. 9, pp. 6099-6111, Sept. 2019.

[27] W. K. Xu, L. Wang, and G. Kolumbán, "A novel differential chaos shift keying modulation scheme," *Int. J. Bifurcation Chaos*, vol. 21, no. 3, pp. 799-814, Mar. 2011.

[28] G. Kaddoum, M. F. A. Ahmed and Y. Nijsure, "Code index modulation: A high data rate and energy efficient communication system," *IEEE Commun. Lett.*, vol. 19, no. 2, pp. 175-178, Feb. 2015.

[29] G. Kaddoum, Y. Nijsure and H. Tran, "Generalized code index modulation technique for high-data-rate communication systems," *IEEE Trans. Veh. Technol.*, vol. 65, no. 9, pp. 7000-7009, Sept. 2016.

[30] W. Xu, L. Wang, and G. Kolumbán, "A new data rate adaption communications scheme for code-shifted differential chaos shift keying modulation," *Int. J. Bifurcation Chaos*, vol. 22, no. 8, pp. 1-8, 2012.

[31] G. Kaddoum, E. Soujeri and Y. Nijsure, "Design of a short reference noncoherent chaos-based communication systems," *IEEE Trans. Commun.*, vol. 64, no. 2, pp. 680-689, Feb. 2016.

[32] H. Yang, W. K. S. Tang, G. Chen, and G.-P. Jiang, "System design and performance analysis of orthogonal multi-level differential chaos shift keying modulation scheme," *IEEE Trans. Circuits Syst. I, Reg. Papers*, vol. 63, no. 1, pp. 146-156, Jan. 2016.

[33] W. Xu, T. Huang and L. Wang, "Code-shifted differential chaos shift keying with code index modulation for high data rate transmission," *IEEE Trans. Commun.*s, vol. 65, no. 10, pp. 4285-4294, Oct. 2017.

[34] W. Xu, Y. Tan, F. C. M. Lau and G. Kolumbán, "Design and optimization of differential chaos shift keying scheme with code index modulation," *IEEE Trans. Commun.*, vol. 66, no. 5, pp. 1970-1980, May 2018.

[35] X. Cai, W. Xu, D. Wang, S. Hong and L. Wang, "An M-ary orthogonal multilevel differential chaos shift keying system with code index modulation," *IEEE Trans. Commun.*, vol. 67, no. 7, pp. 4835-4847, July 2019.

[36] G. Cai, Y. Fang, J. Wen, S. Mumtaz, Y. Song and V. Frascolla, "Multi-carrier M-ary DCSK system with code index modulation: An efficient solution for chaotic communications," *IEEE J. Sel. Topics Signal Process.*, vol. 13, no. 6, pp. 1375-1386, Oct. 2019.

[37] X. Cai, W. Xu, L. Wang and G. Kolumbán, "Multicarrier M-ary orthogonal chaotic vector shift keying with index modulation for high data rate transmission," *IEEE Trans. Commun.*, vol. 68, no. 2, pp. 974-986, Feb. 2020.

[38] X. Cai, W. Xu, L. Wang and G. Chen, "Towards high-data-rate noncoherent chaotic communication: A multiple-mode differential chaos shift keying system," *IEEE Trans. Wireless Commun.*, vol. 20, no. 8, pp. 4888-4901, Aug. 2021.

[39] X. Cai, W. Xu, F. C. M. Lau and L. Wang, "Joint carrier-code index modulation aided M-ary differential chaos shift keying system," *IEEE Trans. Veh. Technol.*, vol. 69, no. 12, pp. 15486-15499, Dec. 2020.

[40] G. Cheng, L. Wang, W. Xu and G. Chen, "Carrier index differential chaos shift keying modulation," *IEEE Trans. Circuits Syst., II, Exp. Briefs*, vol. 64, no. 8, pp. 907-911, Aug. 2017.

[41] G. Cheng, L. Wang, Q. Chen and G. Chen, "Design and performance analysis of generalised carrier index M-ary differential chaos shift keying modulation," *IET Commun.*, vol. 12, no. 11, pp. 1324-1331, June 2018.

[42] G. Cheng, X. Chen, W. Liu and W. Xiao, "GCI-DCSK: Generalized carrier index differential chaos shift keying modulation," *IEEE Commun. Lett.*, vol. 23, no. 11, pp. 2012-2016, Nov. 2019.

[43] E. Başar, Ü. Aygölü, E. Panayırcı and H. V. Poor, "Orthogonal frequency division multiplexing with index modulation," *IEEE Trans Signal Process.*, vol. 61, no. 22, pp. 5536-5549, Nov.15, 2013.

[44] A. Papoulis, *Probability, Random Variables, and Stochastic Processes*. New York, NY, USA: McGraw-Hill, 1991.

[45] G. Kaddoum and E. Soujeri, "NR-DCSK: A noise reduction differential chaos shift keying system," *IEEE Trans. Circuits Syst. II, Exp. Briefs*, vol. 63, no. 7, pp. 648-652, July 2016.

[46] W. Rao, L. Zhang, Z. Zhang and Z. Wu, "Noise-suppressing chaos generator to improve BER for DCSK systems," in *2017 IEEE International Conference on Communications (ICC)*, Paris, 2017, pp. 1-6.

[47] M. K. Simon and M.-S. Alouini, *Digital Communication Over Fading Channels*, vol. 95, 2nd ed. Newark, NJ, USA: Wiley, 2005.

Xiangming Cai received the B.Eng degree in Information Engineering from Guangdong University of Technology, Guangzhou, China, in 2017. He is currently pursuing the Ph.D. degree with the Department of Information and Communication Engineering, Xiamen University, Xiamen, China. His research interests include chaos-based digital communications, chaotic secure communications and their applications to wireless communications.

Weikai Xu (Member, IEEE) received the B.S. degree in electronic engineering from Three Gorges College, Chongqing, China, in 2000, the M.Sc. degree in communication and information system from the Chongqing University of Posts and Telecommunications, Chongqing, China, in 2003, and the Ph.D. degree in electronic circuit and system from the Xiamen University of China, Xiamen, China, in 2011. From 2003 to 2012, he was a Teaching Assistant, and Assistant Professor with the Department of Communication Engineering, Xiamen University. He is now an Associate Professor with the department of Information and Communication Engineering, Xiamen University. His research interests include chaotic communications, underwater acoustic communications, channel coding, cooperative communications and ultra-wideband.

Shaohua Hong (Member, IEEE) received the B.Sc. degree in electronics and information engineering and the Ph.D. degree in electronics science and technology from Zhejiang University, Hangzhou, China, in 2005 and 2010, respectively. He is currently an Associate Professor with the Department of Information and Communication Engineering, Xiamen University, Xiamen, China. He is also an Associate Professor with the Shenzhen Research Institute, Xiamen University, Shenzhen, China. His research interests include joint source and channel coding, wireless communication, and image processing. He has been serving as an Editor for the *KSII Transactions on Internet and Information Systems* since 2015.

Lin Wang (Senior Member, IEEE) received the M.Sc. degree in applied mathematics from the Kunming University of Technology, China, in 1988, and the Ph.D. degree in electronics engineering from the University of Electronic Science and Technology of China, China, in 2001. From 1984 to 1986, he was a Teaching Assistant with the Mathematics Department, Chongqing Normal University. From 1989 to 2002, he was a Teaching Assistant, a Lecturer, and then an Associate Professor in applied mathematics and communication engineering with the Chongqing University of Post and Telecommunication, China. From 1995 to 1996, he was with the Mathematics Department, University of New England, Armidale, NSW, Australia, for one year. In 2003, he was a Visiting Researcher with the Center for Chaos and Complexity Networks, Department of Electronic Engineering, City University of Hong Kong, for three months. In 2013, he was a Senior Visiting Researcher with the Department of ECE, University of California at Davis, Davis, CA, USA. From 2003 to 2012, he was a Full Professor and an Associate Dean with the School of Information Science and Engineering, Xiamen University, China. He has been a Distinguished Professor since 2012. He holds 14 patents in the field of physical layer in digital communications. He has authored over 100 journal and conference papers. His current research interests are in the area of channel coding, joint source and channel coding, chaos modulation, and their applications to wireless communication and storage systems.

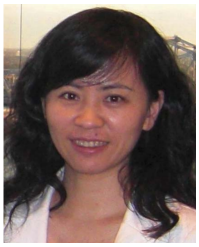

Lin Zhang (Senior Member, IEEE) received the Ph.D. degree in information and communication engineering from Sun Yat-sen University in 2003. In 2003, she joined the School of Information Science and Technology, Sun Yat-sen University, where she has been an Associate Professor since2007. From 2008 to 2009, she was a Visiting Researcher with the Electrical and Computer Engineering Department, University of Maryland, College Park, USA. In 2016, she joined the School of Electronics and Information Technology, Sun Yat-sen University. She is also with the Southern Marine Science and Engineering Guangdong Laboratory. From 2021, she joined School of Information Science and Technology, Tibet University. Her research has been supported by the National Natural Science Foundation of China and the Science and Technology Program Project of Guangdong Province. Her current research interests are in the area of signal processing and their applications to wireless communication systems.